CISLUNAR SPACE DOMAIN AWARENESS USING THE MODIFIED GENERALIZED EQUINOCTIAL ORBITAL ELEMENTS

M. Gupta and K. J. DeMars

Department of Aerospace Engineering, Texas A&M University, College Station, TX 77843 USA, Email:
{maanineegupta, demars}@tamu.edu

ABSTRACT

Cislunar space presents new challenges for Space Domain Awareness (SDA), requiring advanced uncertainty characterization due to complex, non-Keplerian dynamics. The Generalized Equinoctial Orbital Elements (GEqOEs) have been explored as a viable alternative for cislunar dynamical modeling and uncertainty propagation. In this paper, the Modified Generalized Equinoctial Orbital Elements (M-GEqOEs) are introduced for improving robustness in modeling spacecraft dynamics in this regime. Example applications include trajectories that transfer between the Earth and the Moon and families of periodic orbits that span a range of energy levels. Uncertainty evolution is assessed and compared against Cartesian techniques, with the generalized coordinates showing improved accuracy and preserving Gaussian behavior for longer durations.

Keywords: Space Domain Awareness; cislunar astrodynamics; orbital elements.

1. INTRODUCTION

With the recent interest in missions to the vicinity of the Moon, cislunar space is poised to become the domain that sustains humanity's presence beyond the Earth. With this renewed interest, Space Domain Awareness (SDA), that has conventionally applied to the sub-geosynchronous orbit domain, will be necessary to support cooperative and safe operations in cislunar space as well. In contrast to SDA near the vicinity of the Earth, SDA in the broad volume of cislunar space presents unique challenges due to its vast size and significant distance from the Earth. In addition, the cislunar dynamical environment is characterized by non-Keplerian motion resulting from the nonnegligible impact of lunar gravity perturbations. Thus, a dynamical model that captures the influence of both the Earth and the Moon, in addition to other perturbing forces, is necessary to represent cislunar dynamics.

A necessary component of SDA is modeling the uncertainty in the state of a spacecraft and its evolution over time. Assumptions of Gaussianity on the initial and downstream evolution of uncertainty in cislunar space are typically restrictive and do not represent the true behavior. As such, alternative techniques are needed to maintain the Gaussian assumption while preserving uncertainty realism. These techniques are of particular interest in order to obtain and maintain custody of both known and unknown objects in cislunar space. The Alternate Equinoctial Orbital Elements (AEOEs) have been investigated for their preservation of Gaussianity of the initial state uncertainty through propagation under Keplerian motion [7]. The Generalized Equinoctial Orbital Elements (GEqOEs) have been successfully leveraged for the state and uncertainty propagation of near-Earth orbits with third-body perturbations and oblateness effects [2, 6]. By leveraging the GEqOEs, improvement in the preservation of uncertainty realism is demonstrated near the Earth, highlighting their advantages over conventional coordinate representations [9]. More recently, Gupta and DeMars have applied the GEqOEs for capturing three-body dynamical motion in cislunar space, with better preservation of Gaussian behavior for uncertainty propagated along various cislunar orbits [4, 5].

The goal of this investigation is to extend the applicability of the GEqOEs to other cislunar trajectories of interest, including families of periodic orbits that span a variety of energy levels and transfer trajectories that traverse the Earth-Moon corridor. Modifications to the GEqOE set are investigated for robust propagation of cislunar dynamics. As such, the Modified Generalized Equinoctial Orbital Element (M-GEqOE) set is explored as a natural extension within the generalized coordinates. Both the GEqOE and M-GEqOE sets are characterized by the total energy of the system, allowing the direct inclusion of relevant perturbations that arise from conservative forces and providing the necessary framework for modeling non-Keplerian dynamics. Various orbits are constructed using these orbital elements and verified against conventional Cartesian propagation obtained via the Earth-Moon Circular Restricted Three-Body dynamical model.

The first step in addressing the challenges with cislunar SDA is to sufficiently model the relevant dynamical perturbations. The next step is to predict the evolution of uncertainty along a given trajectory and to evaluate the ex-

tent to which it can be accurately characterized in a computationally tractable manner. As such, the uncertainty along various trajectories is propagated in the generalized coordinates and compared against Cartesian propagation techniques. Measures of probability density functions are employed to quantify errors induced by Gaussian approximations of the probability densities in both coordinates.

2. GENERALIZED ORBITAL MOTION

Consider a spacecraft of mass m orbiting the Earth or the Moon. In the associated body-centered inertial frame, the perturbed two-body motion of the spacecraft is represented as

$$\ddot{\boldsymbol{r}} + \frac{\mu_C \boldsymbol{r}}{r^3} = \boldsymbol{a}_p(\boldsymbol{r}, \dot{\boldsymbol{r}}, t) , \tag{1}$$

where $\boldsymbol{r}$ represents the inertial position vector of the spacecraft, $\dot{\boldsymbol{r}}$ is the velocity, and $\ddot{\boldsymbol{r}}$ is the spacecraft acceleration. The vector $\boldsymbol{a}_p$ represents any perturbing accelerations acting on the spacecraft. The variables r and t denote the magnitude of the spacecraft position and time respectively. The parameter μ_C represents the gravitational parameter for the central body (e.g., the Earth or the Moon), where the mass of the spacecraft is assumed to be infinitesimal relative to the mass of the central body.

The origin of the inertial reference frame, denoted O, is centered on the celestial body and is defined as

$$\Sigma = \{O;\ \boldsymbol{e}_x,\ \boldsymbol{e}_y,\ \boldsymbol{e}_z\} . \tag{2}$$

Here, $\boldsymbol{e}_x = [1,\ 0,\ 0]^T$, $\boldsymbol{e}_y = [0,\ 1,\ 0]^T$, and $\boldsymbol{e}_z = [0,\ 0,\ 1]^T$. Additionally, the orbital reference frame, denoted Σ_{or}, is defined by the orthonormal basis,

$$\Sigma_{or} = \{O;\ \boldsymbol{e}_r,\ \boldsymbol{e}_f,\ \boldsymbol{e}_h\} , \tag{3}$$

where $\boldsymbol{e}_r$ points along the spacecraft position vector, $\boldsymbol{e}_h$ is directed along the angular momentum vector, and $\boldsymbol{e}_f$ completes the dextral orthonormal triad

$$\boldsymbol{e}_r = \frac{\boldsymbol{r}}{r}, \quad \boldsymbol{e}_f = \boldsymbol{e}_h \times \boldsymbol{e}_r, \quad \boldsymbol{e}_h = \frac{\boldsymbol{r} \times \dot{\boldsymbol{r}}}{|\boldsymbol{r} \times \dot{\boldsymbol{r}}|} = \frac{\boldsymbol{h}}{h} . \tag{4}$$

The perturbing accelerations in Equation (1) arise from a total perturbing force, denoted $\boldsymbol{F}$, that can be written as a sum of forces that are derived from a potential energy, such as the gravitational acceleration from additional celestial bodies, and forces that are not derived from a potential, such as atmospheric drag and solar radiation pressure. Mathematically, the total perturbing force is then represented as

$$\boldsymbol{F} = \boldsymbol{P} - \nabla U , \tag{5}$$

where $\boldsymbol{P}$ represents the perturbing forces that do not arise from a potential, and $-\nabla U$ models the contribution of forces derived from a potential energy, U. The total orbital energy of the spacecraft, $\mathcal{E}$, is a sum of its Keplerian energy, $\mathcal{E}_K$, and this potential energy, such that

$$\mathcal{E} = \mathcal{E}_K + U . \tag{6}$$

Expressing the spacecraft velocity vector, $\dot{\boldsymbol{r}}$, in the orbital frame as

$$\dot{\boldsymbol{r}} = \dot{r}\boldsymbol{e}_r + \frac{h}{r}\boldsymbol{e}_h , \tag{7}$$

the total orbital energy may be represented as

$$\mathcal{E} = \frac{\dot{r}^2}{2} + \frac{h^2}{2r^2} - \frac{\mu_C}{r} + U , \tag{8}$$

where $\dot{r}$ denotes the radial component of the velocity, and h is the magnitude of the angular momentum of the spacecraft. Then, the effective potential energy, denoted U_{eff}, is defined as

$$U_{\text{eff}} = \frac{h^2}{2r^2} + U . \tag{9}$$

Thus, the total energy of the spacecraft is

$$\mathcal{E} = \frac{\dot{r}^2}{2} - \frac{\mu_C}{r} + U_{\text{eff}} . \tag{10}$$

Using the effective potential energy, the *generalized* angular momentum of the spacecraft, denoted $\tilde{h}$, is introduced,

$$\tilde{h} = \sqrt{2r^2 U_{\text{eff}}} \tag{11}$$

which defines the *generalized* velocity vector

$$\tilde{\boldsymbol{v}} = \dot{r}\boldsymbol{e}_r + \frac{\tilde{h}}{r}\boldsymbol{e}_h . \tag{12}$$

Parameters denoted by tildes represent generalized quantities that are defined by the total orbital energy, $\mathcal{E}$, and are, thus, embedded with conservative perturbations acting on the spacecraft. Although this framework is described in the context of orbits centered on the Earth or the Moon, the equations are applicable to orbits centered on other bodies as well.

2.1. Generalized Equinoctial Orbital Elements

Assuming that the total energy is negative, the generalized analogs for the semi-major axis, eccentricity, and the semi-latus rectum are evaluated as

$$\tilde{a} = -\frac{\mu_C}{2\mathcal{E}} \tag{13}$$

$$\tilde{e} = \frac{\sqrt{\mu_C^2 + 2\mathcal{E}\tilde{h}^2}}{\mu_C} \tag{14}$$

$$\tilde{p} = \tilde{a}(1 - \tilde{e}^2) . \tag{15}$$

The generalized eccentricity vector, $\tilde{\boldsymbol{e}}$, orients the ellipse in the orbital plane and is given as

$$\mu_C \tilde{\boldsymbol{e}} = \tilde{\boldsymbol{v}} \times (\boldsymbol{r} \times \tilde{\boldsymbol{v}}) - \mu_C \boldsymbol{e}_r . \tag{16}$$

The generalized true anomaly, $\tilde{\theta}$, defines the angle between the $\tilde{\boldsymbol{e}}$ and $\boldsymbol{r}$ vectors and satisfies the relations

$$\tilde{e}\cos\tilde{\theta} = \frac{\tilde{h}^2}{\mu_C r} - 1 \tag{17}$$

$$\tilde{e}\sin\tilde{\theta} = \frac{\tilde{h}\dot{r}}{\mu_C} . \tag{18}$$

Other angular relationships that parameterize the non-osculating ellipse include the classical true longitude

$$L = \omega + \Omega + \theta \,, \qquad (19)$$

where θ is the classical true anomaly, and ω and Ω denote the argument of periapsis and the right ascension of ascending node, respectively. The angle Ψ denotes the generalized longitude of periapsis and is determined as

$$\Psi = L - \tilde{\theta} = \omega + \Omega + \theta - \tilde{\theta} \,. \qquad (20)$$

In the absence of orbital perturbations ($U = 0$), the generalized and classical true anomalies are equal, and $\Psi = \omega + \Omega$.

Using the generalized quantities that characterize the orbital motion and the angular relationships, the Generalized Equinoctial Orbital Elements (GEqOEs) are defined as

$$\{\tilde{n}, \ p_1, \ p_2, \ q_1, \ q_2, \ \tilde{\lambda}\} \,. \qquad (21)$$

The first element denotes the generalized mean motion and is expressed as

$$\tilde{n} = \frac{1}{\mu_C}(-2\mathcal{E})^{3/2} \,. \qquad (22)$$

The second and third elements parameterize the eccentricity vector and are defined as

$$p_1 = \tilde{e} \sin \Psi \qquad (23)$$
$$p_2 = \tilde{e} \cos \Psi \,. \qquad (24)$$

The elements q_1 and q_2 orient the equinoctial reference frame relative to the inertial reference frame. These elements are functions of the classical inclination, i, and the classical right ascension of the ascending node, Ω, expressed as

$$q_1 = \tan \frac{i}{2} \sin \Omega \qquad (25)$$
$$q_2 = \tan \frac{i}{2} \cos \Omega \,. \qquad (26)$$

Finally, $\tilde{\lambda}$ represents the generalized mean longitude and is a function of the generalized mean anomaly, $\tilde{M}$, and the generalized longitude of periapsis, Ψ:

$$\tilde{\lambda} = \tilde{M} + \Psi \,, \qquad (27)$$

where $\tilde{M}$ is determined by solving Kepler's equation for the generalized quantities

$$\tilde{M} = \tilde{E} - \tilde{e} \sin \tilde{E} \,. \qquad (28)$$

Define the generalized eccentric longitude as

$$\tilde{F} = \tilde{E} + \Psi \,. \qquad (29)$$

Substituting Equations (28) and (29) into Equation (27) yields

$$\begin{aligned}
\tilde{\lambda} &= \tilde{E} - \tilde{e} \sin (\tilde{F} - \Psi) + (\tilde{F} - \tilde{E}) \\
&= \tilde{F} - \tilde{e}(\sin \tilde{F} \cos \Psi - \cos \tilde{F} \sin \Psi) \qquad (30) \\
&= \tilde{F} + p_1 \cos \tilde{F} - p_2 \sin \tilde{F} \,,
\end{aligned}$$

where the definitions of the elements p_1 and p_2 via Equations (23) and (24) provide the relevant substitutions. The GEqOEs are formulated under the assumption that the total energy of the system, $\mathcal{E}$, is negative. This inherently limits their applicability to certain cislunar dynamical structures and energy levels near the Earth and the Moon. Therefore, modifications are required to accommodate non-capture behavior in the presence of significant perturbations.

3. MODIFICATIONS TO THE GENERALIZED EQUINOCTIAL ORBITAL ELEMENT SET

An offshoot of the classical Equinoctial Orbital Elements includes the Modified Equinoctial Orbital Elements, wherein the semi-major axis and mean longitude from the classical set are replaced by the semi-latus rectum and the true longitude [14]. In the current work, the same modification is adopted to extend the applicability of the GEqOEs to all orbit types, defining the Modified Generalized Equinoctial Orbital Elements (M-GEqOEs). The relevant equations and time derivatives of the M-GEqOE set are detailed.

3.1. Modified Generalized Equinoctial Orbital Elements

The set of Modified Generalized Equinoctial Orbital Elements (M-GEqOEs) is defined as

$$\{\tilde{p}, \ p_1, \ p_2, \ q_1, \ q_2, \ L\}, \qquad (31)$$

where only the first and the sixth elements of the original GEqOE set are modified. The first element in the M-GEqOE set is selected as the generalized semi-latus rectum, $\tilde{p}$, determined as

$$\tilde{p} = \frac{\tilde{h}^2}{\mu_C} \,. \qquad (32)$$

The sixth element of this modified set is the classical true longitude, L, which represents the time-varying or "fast" variable along the orbit. The true longitude is directly determined from Equation (19) as a function of the classical true anomaly, the RAAN, and the argument of periapsis.

3.2. M-GEqOE Time Derivatives

The process of obtaining the time derivatives for each element in the GEqOE is detailed by Baù et al. [2]. In this

section, the time derivatives for the modified set are detailed, providing a general form that may accommodate any perturbing forces. From Equation (5), recall that any perturbing force $\boldsymbol{F}$ comprised of conservative perturbations (derived from some potential energy, U) and non-conservative forces may be embedded into the generalized elements. Projections of the total perturbing force and the non-conservative force term, denoted $\boldsymbol{P}$, into the orbital reference frame are given as

$$F_r = \boldsymbol{F} \cdot \boldsymbol{e}_r, \quad F_f = \boldsymbol{F} \cdot \boldsymbol{e}_f \quad \text{and} \quad F_h = \boldsymbol{F} \cdot \boldsymbol{e}_h \quad (33)$$
$$P_r = \boldsymbol{P} \cdot \boldsymbol{e}_r, \quad P_f = \boldsymbol{P} \cdot \boldsymbol{e}_f \quad \text{and} \quad P_h = \boldsymbol{P} \cdot \boldsymbol{e}_h \; . \tag{34}$$

Additionally, the angular velocity of the equinoctial reference frame, Σ_{eq}, with respect to the inertial frame, Σ, is projected onto the equinoctial axes as

$$w_X = F_h \frac{r}{h} \cos L, \tag{35}$$

$$w_Y = F_h \frac{r}{h} \sin L, \tag{36}$$

$$w_Z = -F_h \frac{r}{h} \tan \frac{i}{2} \sin \omega + \theta \; . \tag{37}$$

Other quantities necessary to compute the time derivatives of the M-GEqOEs include the rate of change of the total energy of the system, that is evaluated as

$$\dot{\mathcal{E}} = \frac{\partial U}{\partial t} + \dot{r} P_r + \frac{h}{r} P_f \; . \tag{38}$$

Then, the general form of the time derivatives of the M-GEqOEs is given as

$$\dot{\tilde{p}} = \frac{2\tilde{h}}{\mu_C} \left[\frac{r^2 \dot{\mathcal{E}}}{\tilde{h}} + \frac{r \dot{r}}{\tilde{h}} (2U - r F_r) \right]$$

$$\dot{p}_1 = p_2 \left(\frac{h - \tilde{h}}{r^2} - w_h \right) + \frac{1}{\tilde{h}} \left(\frac{X}{\tilde{a}} + 2 p_2 \right) (2U - r F_r)$$

$$\quad + \frac{1}{\tilde{h}^2} \left[Y(r + \tilde{p}) + r^2 p_1 \right] \dot{\mathcal{E}}$$

$$\dot{p}_2 = p_1 \left(w_h - \frac{h - \tilde{h}}{r^2} \right) - \frac{1}{\tilde{h}} \left(\frac{Y}{\tilde{a}} + 2 p_1 \right) (2U - r F_r)$$

$$\quad + \frac{1}{\tilde{h}^2} \left[X(r + \tilde{p}) + r^2 p_2 \right] \dot{\mathcal{E}}$$

$$\dot{q}_1 = \frac{1}{2} w_Y \left(1 + q_1^2 + q_2^2 \right)$$

$$\dot{q}_2 = \frac{1}{2} w_X \left(1 + q_1^2 + q_2^2 \right)$$

$$\dot{L} = \frac{h}{r^2} + \frac{r}{h} F_h \tan \left(\frac{i}{2} \right) \sin \left(\omega + \theta \right) \; . \tag{39}$$

Any significant perturbations, whether conservative or non-conservative, that are essential for modeling spacecraft dynamics are, thus, directly incorporated into the generalized elements and their time derivatives.

4. CISLUNAR DYNAMICS MODELING

As spacecraft and other objects traverse cislunar space, their complex dynamical motion is influenced by the gravitational forces of both the Earth and the Moon. Therefore, in addition to the dominant gravitational influence of one body, the gravitational perturbation caused by the other must be accounted for in trajectory design and prediction. While other perturbations, such as the oblateness effects of the Earth and Moon or the gravitational influence of the Sun, may also be significant, accounting for the gravitational forces of both the Earth and the Moon is essential. For cislunar state propagation employing the the M-GEqOEs, the process of incorporating conservative perturbations that arise from third-body gravity effects is summarized. Additionally, the Earth-Moon Circular Restricted Three-Body Problem (CR3BP), a dynamical model based in Cartesian coordinates that serves as an analog to the generalized methodology, is briefly introduced.

4.1. Generalized Coordinates

Cislunar trajectories are parameterized in the generalized coordinates by embedding third-body gravity perturbations. A general form of the potential energy associated with the perturbing force is given as [1]

$$U_P = \mu_P \left(\frac{1}{r_{Psc}} - \frac{\boldsymbol{r} \cdot \boldsymbol{r}_{CP}}{r_{CP}^3} \right) , \tag{40}$$

where $\boldsymbol{r}$ represents the position vector from the central body to the spacecraft, and the subscripts C and P represent the central and perturbing bodies, respectively. Equation (40) may be rewritten as a convergent series of Legendre polynomials

$$U_P = \frac{\mu_P}{r_{CP}} \left[1 + \sum_{k=2}^{k=\infty} \left(\frac{r}{r_{CP}} \right)^k P_k(\cos \alpha) \right] , \tag{41}$$

where α is the angle between the position vectors $\boldsymbol{r}$ and $\boldsymbol{r}_{CP}$, and P_k represent Legendre polynomials [1]. The perturbing acceleration takes the form

$$-\nabla U_P = \frac{\mu_P}{r_{CP}^2} \sum_{k=1}^{k=\infty} \left(\frac{r}{r_{CP}} \right)^k \tag{42}$$

$$\times \left[P_{k+1}'(\cos \alpha) \boldsymbol{e}_{\boldsymbol{r}_{CP}} - P_k'(\cos \alpha) \boldsymbol{e}_{\boldsymbol{r}} \right] , \tag{43}$$

where $\boldsymbol{e}_{\boldsymbol{r}_{CP}}$ and $\boldsymbol{e}_{\boldsymbol{r}}$ are the unit vectors along $\boldsymbol{r}_{CP}$ and $\boldsymbol{r}$ respectively. By embedding the third-body potential energy directly into the total energy of the system, leveraging the time derivatives of the M-GEqOEs, the element set is numerically integrated to obtain the spacecraft state history over time. Furthermore, after integration, the M-GEqOE set is transformed into Cartesian coordinates at each time step to obtain a direct comparison against the conventional CR3BP solutions.

4.2. Cartesian Coordinates

One dynamical model that serves as a point of comparison against third-body perturbed M-GEqOE solutions is the CR3BP. The Earth-Moon CR3BP is a medium-fidelity dynamical model that takes into account the gravity of Earth and Moon on the motion of the spacecraft [12]. The third body, assumed to be a massless spacecraft, does not influence the orbits of the Earth and the Moon, which orbit their mutual barycenter in circular coplanar orbits. The CR3BP adopts a rotating frame based in the motion of the primary bodies to describe the behavior of the spacecraft governed by the Earth and the Moon. In this frame, represented $\{^R\hat{\boldsymbol{x}}, \ ^R\hat{\boldsymbol{y}}, \ ^R\hat{\boldsymbol{z}}\}$, $^R\hat{\boldsymbol{x}}$ is directed from the Earth to the Moon, $^R\hat{\boldsymbol{z}}$ is parallel to the angular momentum direction of the system, and $^R\hat{\boldsymbol{y}}$ completes the dextral orthonormal triad. The quantities l^*, m^*, and t^*, termed the characteristic length, characteristic mass, and characteristic time, respectively, nondimensionalize the equations of motion that govern the motion of the spacecraft. The resulting scalar equations of motion, expressed in the rotating frame, are

$$\ddot{x} - 2\dot{y} = \frac{\partial U^*_{\text{CR3BP}}}{\partial x}, \tag{44}$$

$$\ddot{y} + 2\dot{x} = \frac{\partial U^*_{\text{CR3BP}}}{\partial y}, \tag{45}$$

$$\ddot{z} = \frac{\partial U^*_{\text{CR3BP}}}{\partial z} . \tag{46}$$

The quantity U^*_{CR3BP} is a pseudo-potential function defined as

$$U^*_{\text{CR3BP}} = \frac{1 - \mu_{\text{CR3BP}}}{r_{Esc}} + \frac{\mu_{\text{CR3BP}}}{r_{Msc}} + \frac{x^2 + y^2}{2} , \tag{47}$$

where μ_{CR3BP} is the CR3BP system mass parameter evaluated as

$$\mu_{\text{CR3BP}} = \frac{M_M}{M_E + M_M} , \tag{48}$$

where the quantities M_E and M_M represent the mass of the Earth and the Moon, respectively. For the Earth-Moon system, this value is approximately equal to $\mu_{\text{CR3BP}} = 0.0121506$. Note that in Equation (47), r_{Esc} and r_{Msc} denote the nondimensionalized distances between the Earth and the spacecraft as well as the Moon and the spacecraft, respectively. The values $[x, \ y, \ z]$ correspond to the nondimensional position of the spacecraft relative to the system barycenter in the Earth-Moon rotating frame; similarly, $[\dot{x}, \ \dot{y}, \ \dot{z}]$ represent the velocity components of the spacecraft as viewed in the rotating frame. The CR3BP permits one integral of motion, termed the Jacobi constant, which provides insight into the energy levels of trajectories within this model. The Jacobi constant is evaluated as

$$C = 2U^*_{\text{CR3BP}} - (\dot{x}^2 + \dot{y}^2 + \dot{z}^2) . \tag{49}$$

For additional insight into the evolution of various cislunar trajectories, solutions from the CR3BP that are inherently based in the Earth-Moon rotating frame are transformed into inertial frames centered on either primary body.

5. UNCERTAINTY PROPAGATION

The current work employs two methods for propagating the uncertainty associated with each cislunar orbit. With some given initial mean and covariance, the uncertainties are evolved for multiple revolutions to illustrate their characterization over both short and long time horizons.

5.1. Monte Carlo Analysis

Monte Carlo analysis is employed to obtain a representation of the *true* probability distribution along the orbit in both Cartesian and generalized coordinates. In the current work, $N = 10,000$ samples are utilized for all simulations to facilitate preliminary analysis while maintaining computational feasibility. For uncertainty propagated in Cartesian coordinates, the N samples are propagated using the CR3BP equations of motion for a given propagation time. Similarly, the M-GEqOE equations of motion embedded with third-body gravity perturbations are propagated for N samples for the same total propagation time. At each time step, then, the mean and covariance for either scenario are computed as

$$\boldsymbol{m}(t) = \frac{1}{N} \sum_{i=1}^{N} \boldsymbol{x}_i(t) \tag{50}$$

$$\boldsymbol{P}(t) = \frac{1}{N} \sum_{i=1}^{N} (\boldsymbol{x}_i(t) - \boldsymbol{m}(t)) (\boldsymbol{x}_i(t) - \boldsymbol{m}(t))^T , \tag{51}$$

where $\boldsymbol{x}_i(t)$ is the state of the ith sample at time t. The mean and covariance computed via Monte Carlo methods serve as a benchmark for comparing other approaches that aim to approximate these statistical moments.

5.2. Unscented Transform

The Unscented Transform (UT) is a methodology for deterministically sampling a fixed number of points, termed sigma points, to approximate the mean and covariance of some given distribution [8]. Consider some nonlinear transformation represented as

$$\boldsymbol{y} = \boldsymbol{g}(\boldsymbol{x}) , \tag{52}$$

where $\boldsymbol{x}$ is Gaussian. The mean and covariance of $\boldsymbol{x}$ are known and denoted as $\boldsymbol{m}_x$ and $\boldsymbol{P}_{xx}$, respectively. The pdf of $\boldsymbol{x}$ is, thus, expressed as $p(\boldsymbol{x}) = p_g(\boldsymbol{x}; \boldsymbol{m}_x, \boldsymbol{P}_{xx})$. The goal of the UT is to approximate the mean and covariance of $\boldsymbol{y}$, denoted $\boldsymbol{m}_y$ and $\boldsymbol{P}_{yy}$, respectively. Assuming $\boldsymbol{x} \in \mathbb{R}^n$, $2n+1$ sigma points are drawn and given as

$$\boldsymbol{\mathcal{X}}^{(0)} = \boldsymbol{m}_x \tag{53}$$

$$\boldsymbol{\mathcal{X}}^{(i)} = \boldsymbol{m}_x + \sqrt{n + \lambda} \left[\boldsymbol{S}_{xx}\right]_i \tag{54}$$

$$\boldsymbol{\mathcal{X}}^{(i+n)} = \boldsymbol{m}_x - \sqrt{n + \lambda} \left[\boldsymbol{S}_{xx}\right]_i , \tag{55}$$

where $i = 1, ..., n$ [15]. The quantity $[\boldsymbol{S}_{xx}]_i$ is the ith column of the matrix $\boldsymbol{S}_{xx}$, determined such that $\boldsymbol{P}_{xx} = \boldsymbol{S}_{xx}\boldsymbol{S}_{xx}^T$. In this investigation, the Cholesky decomposition is employed to determine this square root factor. The scaling parameter λ is computed as

$$\lambda = \alpha^2 (n + \kappa) - n , \qquad (56)$$

where α and κ dictate the spread of the sigma points around the mean [13]. Once the sigma points are determined, the mean and covariance weights associated with each point are computed

$$w_m^{(0)} = \frac{\lambda}{n + \lambda} \qquad (57)$$

$$w_m^{(i)} = \frac{1}{2(n + \lambda)} \qquad (58)$$

$$w_c^{(0)} = \frac{\lambda}{n + \lambda} + \left(1 - \alpha^2 + \beta\right) \qquad (59)$$

$$w_c^{(i)} = \frac{1}{2(n + \lambda)} \qquad (60)$$

$\forall\, i = 1, ..., 2n$. The subscripts m and c denote the mean and covariance weights respectively. The parameter β is used to incorporate prior information and is optimally set equal to two when the prior is Gaussian [8]. The non-linear transformation in Equation (52) is then applied to each sigma point, yielding the transformed sigma points

$$\boldsymbol{\mathcal{Y}}^{(i)} = \boldsymbol{g}\big(\boldsymbol{\mathcal{X}}^{(i)}\big) , \qquad (61)$$

where $i = 0, ..., 2n$. Together with the mean and covariance weights, the transformed sigma points are used to approximate the mean and covariance as

$$\boldsymbol{m}_y \cong \sum_{i=0}^{2n} w_m^{(i)} \boldsymbol{\mathcal{Y}}^{(i)} \qquad (62)$$

$$\boldsymbol{P}_{yy} \cong \sum_{i=0}^{2n} w_c^{(i)} \big(\boldsymbol{\mathcal{Y}}^{(i)} - \boldsymbol{m}_y\big)\big(\boldsymbol{\mathcal{Y}}^{(i)} - \boldsymbol{m}_y\big)^T . \qquad (63)$$

The UT is employed to transform the initial uncertainty from Cartesian to generalized coordinates [2, 6]. The transformed sigma points are then propagated to approximate the mean and covariance at later times. For this investigation, $n = 6$, and the values of the user-defined parameters are selected as $\alpha = 1$, $\kappa = -3$, and $\beta = 2$.

5.3. Kullback-Leibler Divergence

The Kullback-Leibler divergence is a employed to compare the true distributions obtained via Monte Carlo analysis against the Gaussian approximated distributions obtained via the UT approach. Although the assumption of Gaussianity may not hold for cislunar orbits over time, this measure offers insight into the magnitude of error introduced by a Gaussian approximation. Also called the

relative entropy, the KL divergence is a measure of the informational distance between two distributions $p(\boldsymbol{x})$ and $q(\boldsymbol{x})$, and is determined as [3]

$$D_{KL}[p||q] = \int p(\boldsymbol{x}) \log \frac{p(\boldsymbol{x})}{q(\boldsymbol{x})} \mathrm{d}\boldsymbol{x} . \qquad (64)$$

The KL divergence is positive and goes to zero when the two distributions coincide. For the current work, $p(\boldsymbol{x})$ represents the true distribution, and the pdf $q(\boldsymbol{x})$ represents the Gaussian approximation characterized by mean $\boldsymbol{m}$ and covariance $\boldsymbol{P}$.

To determine the KL divergence, the entropy of the true distribution is employed, defined as

$$h[p] = \mathbb{E}\left\{\log \frac{1}{p(\boldsymbol{x})}\right\} = \int p(\boldsymbol{x}) \log \frac{1}{p(\boldsymbol{x})} \mathrm{d}\boldsymbol{x} . \qquad (65)$$

Using the definition of entropy, the standard form of the KL divergence given in Equation (64) is rewritten as

$$D_{KL}[p||q] = -h[p] - \mathbb{E}_{p(\boldsymbol{x})}\{\log q(\boldsymbol{x})\} , \qquad (66)$$

where $q(\boldsymbol{x}) = p_g(\boldsymbol{x}; \boldsymbol{m}, \boldsymbol{P})$. The equation simplifies to

$$D_{KL}[p||q] = -h[p] + \frac{1}{2} \log |2\pi\boldsymbol{P}| \qquad (67)$$

$$+ \frac{1}{2}\mathbb{E}_{p(\boldsymbol{x})}\left\{(\boldsymbol{x} - \boldsymbol{m})^T \boldsymbol{P}^{-1}(\boldsymbol{x} - \boldsymbol{m})\right\} . \qquad (68)$$

This measure provides insight into the error introduced by approximating the true distribution as a Gaussian distribution. The KL divergence is computed independently for uncertainty propagated in both generalized and Cartesian coordinates.

6. RESULTS AND DISCUSSION

The methodology for propagating cislunar dynamics and uncertainty in the generalized coordinates using the M-GEqOE equations in Equation (39) is demonstrated for various transfer trajectories and periodic orbits of interest. The transfer trajectories that pass from the near-Earth to the lunar region are constructed with the Earth as the central body, and the gravity of the Moon is incorporated as the third-body perturbation via Equation (40). For the selected periodic orbit families that lie near the lunar vicinity, the Moon is selected as the central body, with the gravity of the Earth embedded via Equation (40).

6.1. Lunar Free Return Trajectories

Lunar free returns are trajectories that transfer from the Earth to the lunar vicinity and, without requiring any propulsive maneuvers, return to the vicinity of the Earth [11]. These trajectories were first investigated in the

Apollo era as a means to guarantee a safe return to the Earth in case of emergencies or communications disruptions. Since these trajectories represent pathways for rapid access between the Earth and the Moon, it is crucial to be able to accurately model the underlying dynamics in the generalized coordinates. As such, representative cislunar free return trajectories are investigated in the current work.

Representations of lunar free returns from the Earth-Moon CR3BP are leveraged to assess the accuracy of modeling the dynamics using the M-GEqOEs [10]. Two sample free return trajectories are selected, characterized by cislunar perilune passages and perilune altitudes of approximately $49,500\ km$ and $17,600\ km$. The trajectories are assumed to depart from an Earth-centered orbit of altitude $180\ km$. The times of flight from the Earth till perilune for the two trajectories are $4.3\ days$ and $5.6\ days$, respectively. Results of propagating the trajectories in Cartesian and generalized coordinates using the CR3BP and M-GEqOE equations, respectively, appear in Figure 1 as viewed in the Earth-Moon rotating and Earth-centered inertial frames. The blue curves represent the M-GEqOE solution, while the orange curves correspond to the trajectory obtained from the Earth-Moon CR3BP. For these representative trajectories that traverse from the near-Earth region to the lunar vicinity, the M-GEqOEs are able to capture the underlying dynamical motion and maintain consistency with the CR3BP solution.

6.2. Periodic Orbit Families

Periodic orbit families identified from the Earth-Moon CR3BP near the lunar vicinity are investigated. In particular, the Low Prograde Orbit (LPO) family centered on the Moon, and the L_1 and L_2 halo orbit families centered on their respective libration points in the rotating frame, are constructed using the M-GEqOE equations. For each orbit family, representative members are selected that span a range of Jacobi constant values (energy levels) and lunar radii. Since each orbit in the family possesses a different period in the rotating frame, a fixed propagation duration of two weeks is employed for each orbit. Members from each orbit family appear in Figures 2 to 4 as viewed in Cartesian and generalized coordinates. Despite the vastly differing geometries and energy levels along the orbits in the families, the M-GEqOE propagator is able to accurately represent the behavior originally modeled in the CR3BP.

To build intuition regarding the M-GEqOE set as it pertains to cislunar trajectories, the evolution of the elements is also considered. Figures 2c, 3c and 4c illustrate the evolution of the M-GEqOEs for each orbit in their respective orbit families, colored by the associated Jacobi constant value, over two weeks of propagation time. Consider the evolutio of the M-GEqOEs for the LPOs, as shown in in Figure 2c. Since motion along these orbits is restricted to the Earth-Moon plane, the elements q_1 and q_2 remain constant and zero for each orbit. As the Jacobi

(a) Earth-Moon rotating frame

(b) Earth-centered inertial frame
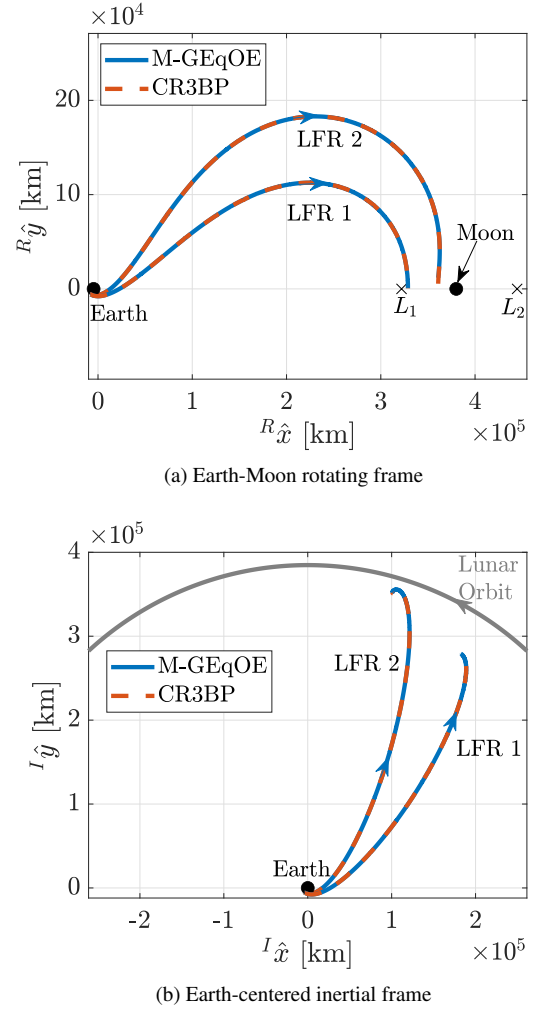
Figure 1. Cartesian representations of sample lunar free return trajectories constructed using the M-GEqEO (blue) and CR3BP (orange) equations.

constant value increases, the orbits become less eccentric, as evident by magnitudes of elements p_1 and p_2 for this family. Similar insight can be gained regarding the geometry and structure of the halo orbit families. Since the halo orbits are inclined relative to the Earth-Moon plane, the elements q_1 and q_2 are no longer zero, with their magnitudes informing the inclination of the respective orbit.
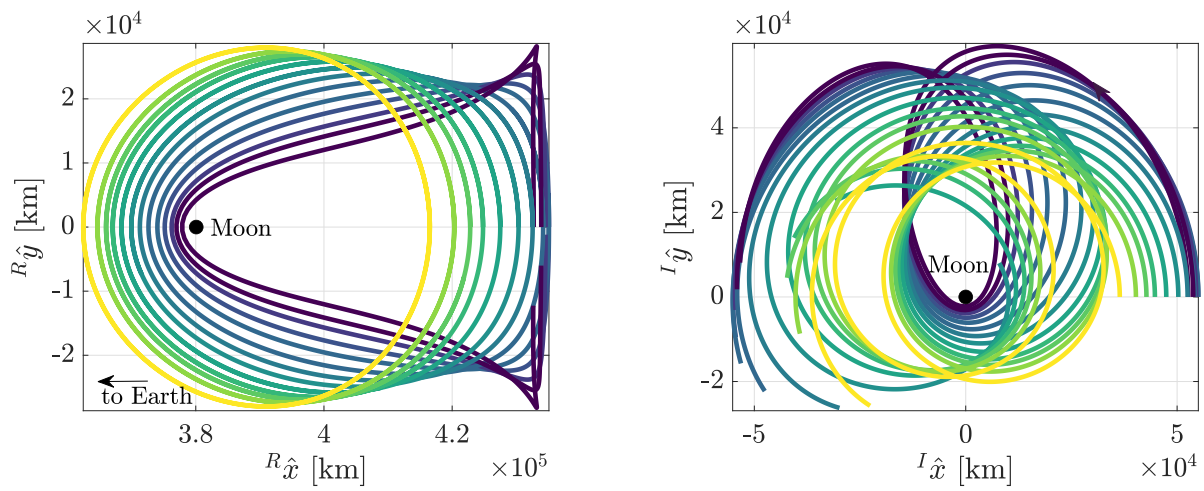
(a) Earth-Moon rotating frame

(b) Moon-centered inertial frame
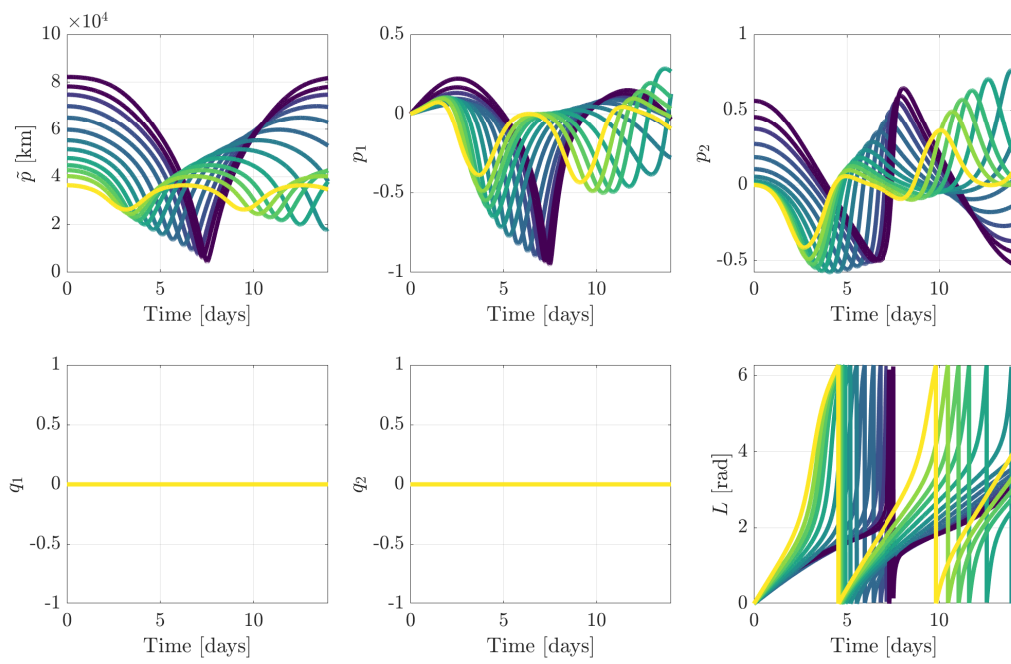
(c) Evolution of M-GEqOEs

Jacobi Constant

*Figure 2. Representative members of the low prograde orbit family constructed using the **M-GEqOE** propagation scheme.*

(a) Earth-Moon rotating frame

(b) Moon-centered inertial frame

(c) Evolution of M-GEqOEs

Jacobi Constant
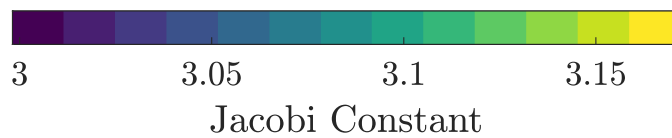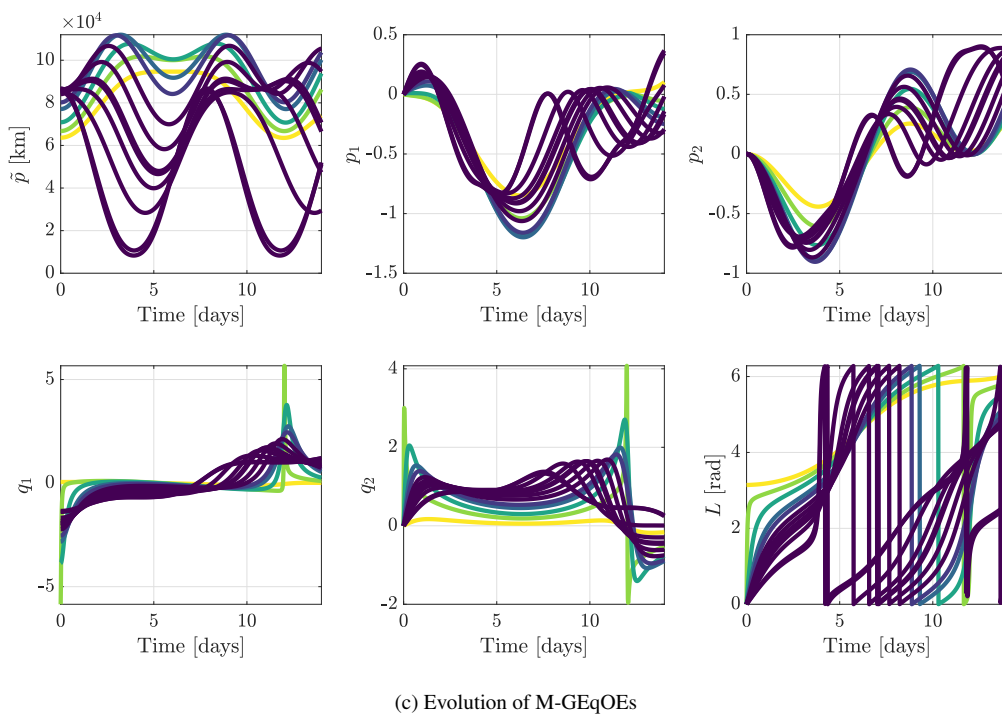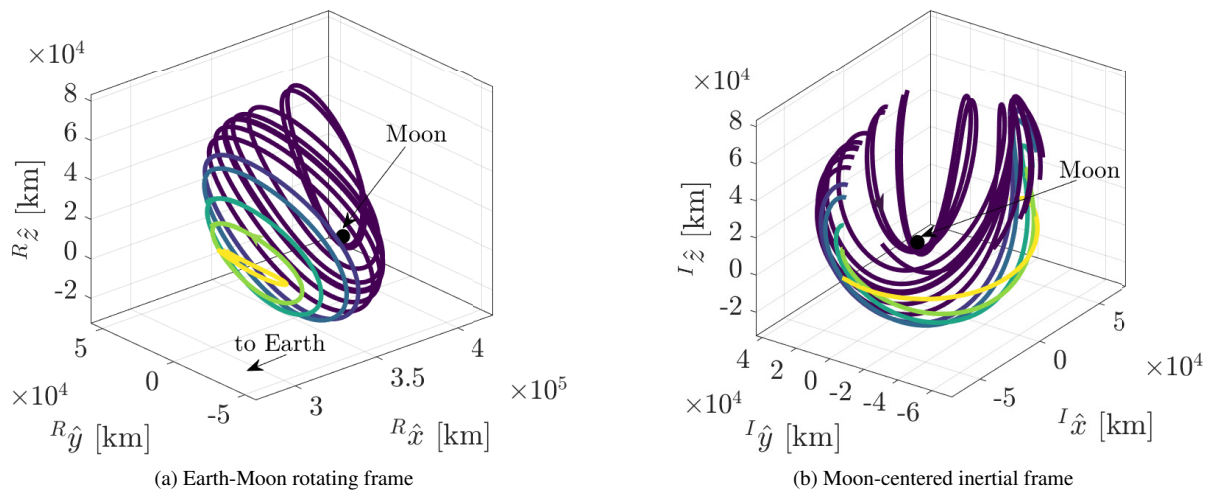
*Figure 3. Representative members of the L_1 halo orbit family constructed using the M-GEqOE propagation scheme.*

(a) Earth-Moon rotating frame

(b) Moon-centered inertial frame

(c) Evolution of M-GEqOEs

Jacobi Constant
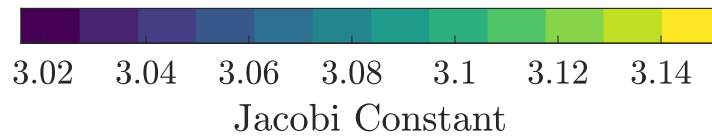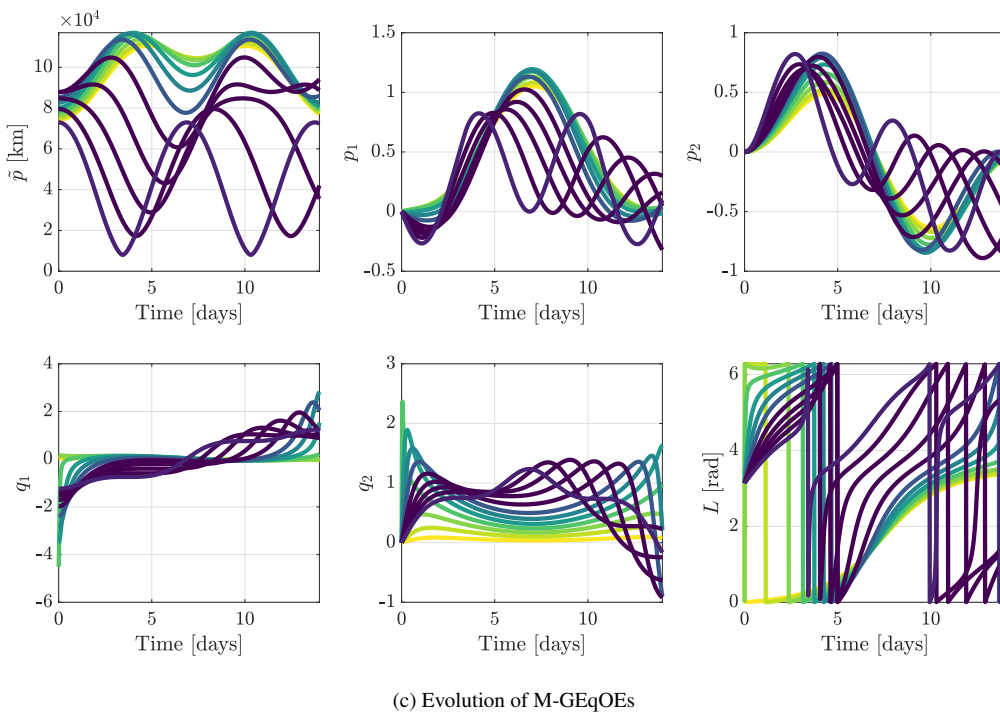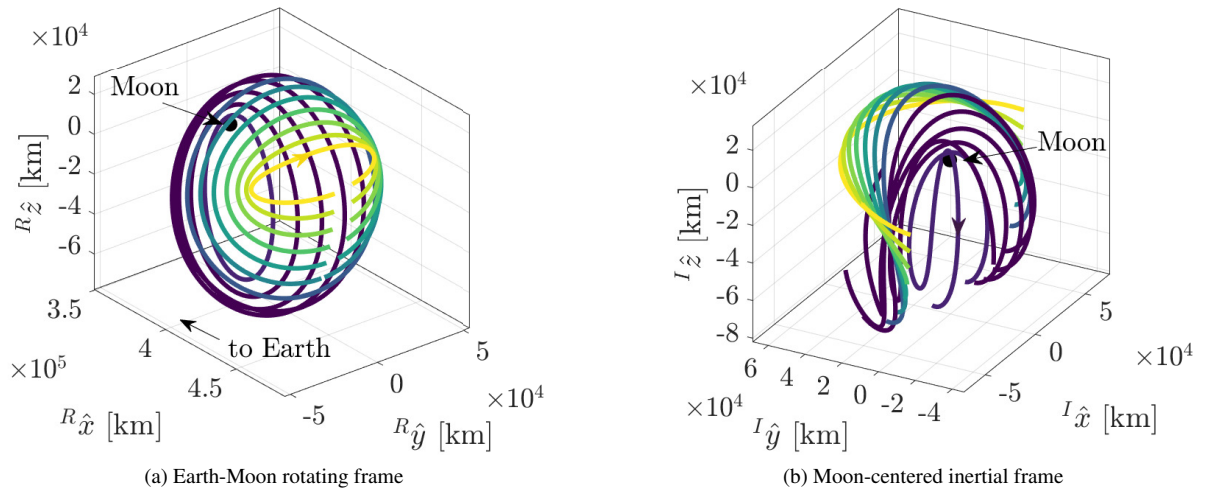
Figure 4. Representative members of the L_2 halo orbit family constructed using the M-GEqOE propagation scheme.

6.3. Uncertainty Propagation

The evolution of uncertainty along cislunar trajectories is demonstrated by evolving the uncertainty in Cartesian and generalized coordinates for the two free return trajectories and a sample LPO. In both sets of coordinates, recall that Monte Carlo analysis provides the true pdf, while a Gaussian approximation is obtained using the Unscented Transform method.

The evolution of the uncertainty along the two lunar free return trajectories is evaluated assuming an initial 1σ uncertainty of $1\ km$ and $0.01\ m/s$ along the position and velocity channels, respectively. The KL divergence is computed for both trajectories with propagation in both coordinate sets, and appears in Figure 5. Notably, even though the uncertainty at initial time is characterized as Gaussian, there is rapid divergence from Gaussian behavior along both sample trajectories. Uncertainty evolved in Cartesian coordinates diverges drastically, whereas propagation via the M-GEqOE set demonstrates better adherence to the Gaussian assumption. It is also noted that there are no immediately apparent regions along the trajectories at which the Gaussian assumption fails. In general, with the M-GEqOE methodology, the likelihood of measurements exhibiting Gaussian behavior is enhanced, ensuring more reliable uncertainty characterization.

In a similar way, the uncertainty growth along the LPO is examined in both coordinates, assuming an initial 1σ value of uncertainty of $10\ km$ and $0.1\ m/s$ along the position and velocity channels. The KL divergence, which quantifies the error introduced by approximating the pdf that characterizes the uncertainty as a Gaussian distribution, is determined for propagation in both coordinates. For propagation initiated at apolune and spanning two weeks, the KL divergence appears in Figure 6. While both methodologies maintain a nominal value of KL divergence, there is an apparent departure from Gaussian behavior exhibited at the $5.7\ day$ mark, which corresponds to passage near perilune. At this location, the uncertainty evolved using the M-GEqOE equations in generalized coordinates exhibits a smaller degree of non-Gaussianity than the Cartesian method, indicating better preservation of uncertainty realism in the generalized coordinates.

This is further validated by projecting the uncertainty cloud obtained via both methodologies along each pair of components that comprise their respective 6-dimensional state, as shown in Figure 7. The lower triangular portion of the pairs plot illustrates uncertainty along Cartesian coordinates, while the upper triangular portion illustrates uncertainty propagated in the generalized coordinates. In each cell of the pairs plot, the gray markers project the Monte Carlo samples along the associated components. For the Cartesian subplots, the black and red curves indicate the 3σ uncertainty intervals associated with the Monte Carlo (true) and UT (approximate) methods, respectively. The mean obtained via Monte Carlo sampling and via the UT is indicated by the black and red markers, respectively, as well. Similarly, in each sub-
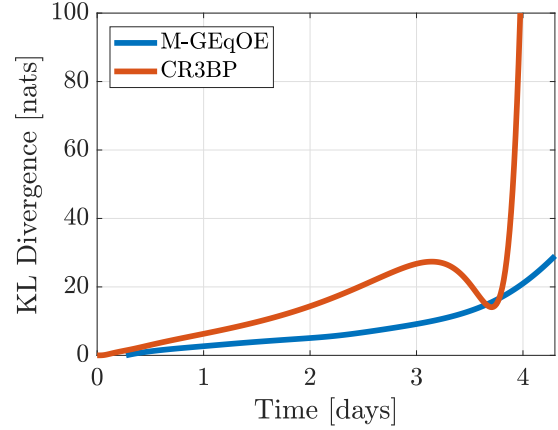
(a) LFR 1
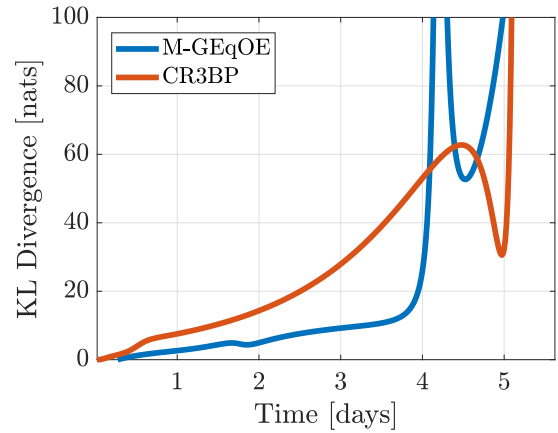
(b) LFR 2

Figure 5. KL divergence between the true and Gaussian approximated distributions that characterize the uncertainty along the sample lunar free return trajectories.
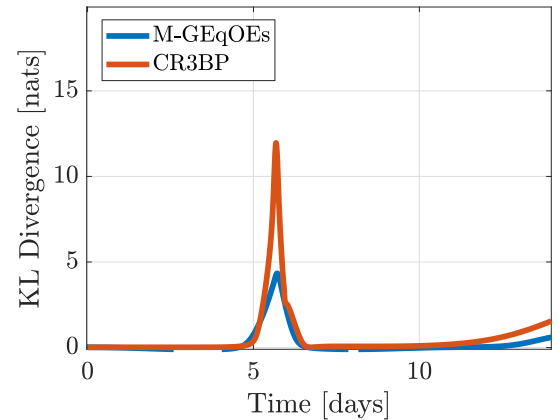

Figure 6. KL divergence between the true and Gaussian approximated distributions for uncertainty propagated along the low prograde orbit.

plot for uncertainty in M-GEqOE coordinates, the black and green curves indicate the 3σ uncertainty intervals associated with the Monte Carlo (true) and UT (approximate) methods, respectively. The black and green markers indicate the true and approximated mean at that time. For the selected LPO, the pairs plot is visualized at the point of the greatest divergence from Gaussian behavior in both coordinates, 5.7 $days$ downstream. At this time, the projections in Cartesian coordinates clearly exhibit non-Gaussian behavior, and the Gaussian approximation supplied by the UT fails to capture a majority of the Monte Carlo samples. In generalized coordinates, non-Gaussian behavior emerges along certain projections that fail to fully capture the tails of the true distribution. However, the overall representation of the distribution remains more accurate compared to the Cartesian approach.

7. CONCLUSIONS

The current work investigates an alternative orbital element representation of cislunar dynamics for applications towards SDA. To overcome the challenges of accurately capturing essential perturbations and to improve uncertainty realism, the Modified Generalized Equinoctial Orbital Element (M-GEqOE) set is introduced. This modified framework relaxes the energy constraints that limit the applicability of the Generalized Equinoctial Orbital Element (GEqOE) set, while preserving the inherent advantages of the latter. The M-GEqOE methodology is implemented for propagating various cislunar transfer trajectories and periodic orbits, showing agreement with the conventional Cartesian solutions. It is also demonstrated that propagating uncertainty directly in generalized coordinates reduces the degree of non-Gaussianity compared to Cartesian uncertainty propagation. At regions along the orbit where uncertainty deviates from Gaussian behavior in Cartesian coordinates, a closer adherence to Gaussianity is observed when propagated using the orbital elements based in the generalized coordinates.

ACKNOWLEDGMENTS

REFERENCES

1. BATTIN, RICHARD H. *An Introduction to the Mathematics and Methods of Astrodynamics*. American Institute of Aeronautics and Astronautics, Reston, VA, 1999.

2. BAÙ, G., HERNANDO-AYUSO, J., AND BOMBARDELLI, C. A Generalization of the Equinoctial Orbital Elements. *Celestial Mechanics and Dynamical Astronomy 133*, 11-12 (Dec. 2021).

3. DUPLANTIER, B., AND RIVASSEAU, V. *Information Theory: Poincaré Seminar 2018*. Progress in Mathematical Physics. Birkhäuser Cham, 2021.

4. GUPTA, M., AND DEMARS, K. J. Cislunar Astrodynamics Leveraging Generalized Equinoctial Orbital Elements. In *AAS/AIAA Space Flight Mechanics Meeting* (Kaua'i, Hawaii, 2025).

5. GUPTA, M., AND DEMARS, K. J. Uncertainty Propagation for Cislunar Space Domain Awareness. In *AAS/AIAA Space Flight Mechanics Meeting* (Kaua'i, Hawaii, 2025).

6. HERNANDO-AYUSO, J., BOMBARDELLI, C., BAÙ, G., AND MARTÍNEZ-CACHO, A. Near-Linear Orbit Uncertainty Propagation Using the Generalized Equinoctial Orbital Elements. *Journal of Guidance, Control, and Dynamics 46*, 4 (2023).

7. HORWOOD, J. T., ARAGON, N. D., AND POORE, A. B. Gaussian Sum Filters for Space Surveillance: Theory and Simulations. *Journal of Guidance, Control, and Dynamics 34*, 6 (2011), 1839–1851.

8. JULIER, S. The Scaled Unscented Transformation. In *Proceedings of the 2002 American Control Conference (IEEE Cat. No.CH37301)* (2002), vol. 6.

9. MCGEE, K. W. State and Uncertainty Propagation using Generalized Equinoctial Orbital Elements. M.S. Thesis, Texas A&M University, College Station, TX, Aug. 2023.

10. PAVLAK, T. A. Mission Design Applications in the Earth-Moon System: Transfer Trajectories and Stationkeeping. M.S. Thesis, Purdue University, West Lafayette, Indiana, 2010.

11. SCHWANIGER, A. J. NASA Technical Note: Trajectories in the Earth-Moon Space with Symmetrical Free Return Properties. *Lunar Flight Study Series* (1963).

12. SZEBEHELY, V. *Theory of Orbits: The Restricted Problem of Three Bodies*. Academic Press Inc., 1967.

13. VAN DER MERWE, R. *Sigma-Point Kalman Filters for Probabilistic Inference in Dynamic State-Space Models*. Ph.D. Dissertation, Oregon Health and Science University, Portland, OR, 2004.

14. WALKER, M. J. H., IRELAND, B., AND OWENS, J. A set of modified equinoctial orbital elements. *Celestial Mechanics 36* (1983), 409–419.

15. ZANETTI, R., AND DEMARS, K. J. Joseph Formulation of Unscented and Quadrature Filters with Application to Consider States. *Journal of Guidance, Control, and Dynamics 36*, 6 (2013), 1860–1864.
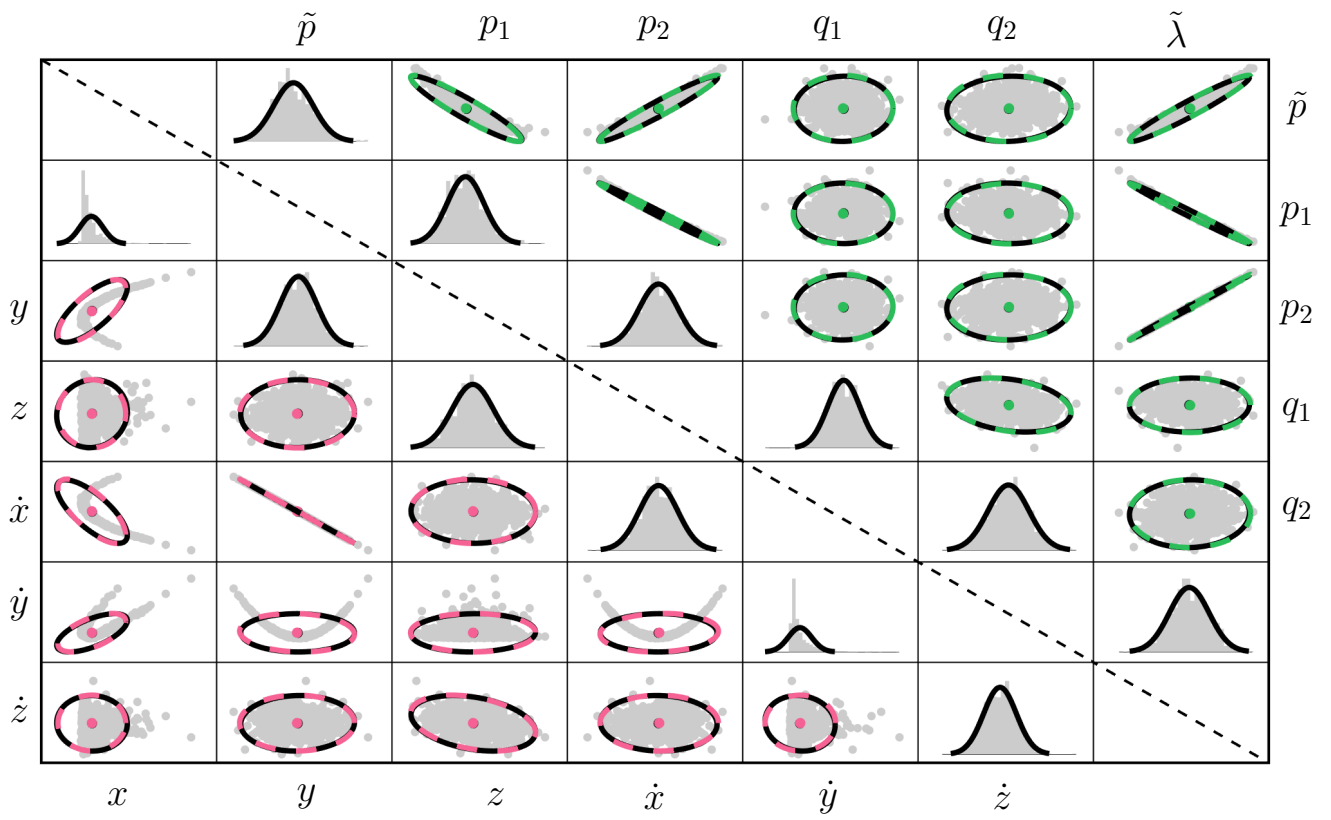
Figure 7. Pairs plot for the LPO at perilune with uncertainty propagated in Cartesian (lower triangular) and generalized (upper triangular) coordinates. Propagation time: 5.7 days.